Journal of the European Ceramic Society **15** (1995) 209–224

0955-2219/95/$9.50

Mechanical Properties of C/SiC Composites as Explained from their Interfacial Features

Jean-François Després & Marc Monthioux

Laboratoire Marcel Mathieu, CNRS-UPPA, Centre Hélioparc, 2 avenue du Président Angot, F64000, Pau, France

(Received 10 March 1994; revised version received 28 June 1994; accepted 1 August 1994)

Abstract

Carbon fibre reinforced ceramic matrix composites with pyrolytic carbon interphases prepared following various conditions are compared, together with interphase-free composites. Four composite grades are thus defined, considering similarities in the ultimate tensile strength and strain values. Textural then structural investigations of the interfacial zones are performed from a centimetric to nanometric scale in an attempt to explain the specific mechanical features of the composites for each grade. Results show that the carbon interphase texture obviously controls the macroscopic behavior of the composites. Composite toughnesses are directly related to the relative strengths of the various interfaces, which depend on the covalent/Van der Waals bond ratio.

1 Introduction

Despite their high ultimate strength or elastic modulus values, monolithic ceramic materials have not been used as structural materials because of their lack of toughness. However, reinforcing them with carbon fibres, which may have both high ultimate strength and Young's modulus values, has allowed tough 2D ceramic matrix composites to be obtained,[1] making them convenient for structural uses in industrial applications.

However, composites only built with carbon fibres as reinforcement within a pure silicon carbide matrix, though reaching higher performances than the monolithic matrix, have a peculiar tensile strength/strain behavior. Considering curve 2 in Fig. 1, three different zones are seen as compared with an unreinforced bulk ceramic material (curve 1). From O to A, the composite exhibits a high elastic modulus value, which depends on the fibre/matrix volume proportions. In A, failures occur in the matrix, because of its lower ultimate strain value compared to the fibres. As failures generalize, multiple fracture of the matrix induces a high strain value, though the increase in strength remains low, resulting in the A—B plateau. In B, the multiple fracture is maximal and the slope of the curve becomes mainly influenced by the fibre modulus, assuming that, as discussed later, the fibre/matrix bonding is weak. The slope of the curve therefore increases (B—C zone). Finally, when the strain-to-failure value of the fibres is reached, fibres quickly break one after the other from C to D. D is the point of final rupture of the sample. The fact that fibres and matrix react successively instead of combining their properties does not provide a good example of the right composite. Such a behavior is specific from a two-component C/SiC composite. Fig.2 gives an example ('interphase-free' curve).

Changing the behavior becomes possible with adding a third component: the interphase (C/C/SiC composites). Fibres are therefore coated with a pyrolytic carbon interphase deposited from a chemical vapor deposition (CVD) process, prior to the densification with the silicon carbide matrix, also from a chemical vapor infiltration (CVI) process. The tensile strength/strain behavior of the resulting composites is now as shown in Fig. 2 ('Grade 3' curve for instance).

However, composites made of the same components (i.e. carbon fibres, pyrolytic carbon interphase, and SiC matrix) may have various ultimate strength and strain values, though coarsly following the same moduli (compare Grade 1, 2, and 3 curves on Fig. 2). Though useful anyway, the efficiency of the pyrocarbon interphase is therefore conditioned by factors other than the chemical nature of the components. The aim of the present paper is to determine these factors.

2 Experimental

All the composites were prepared by the Société Européenne de Propulsion (SEP), the details of

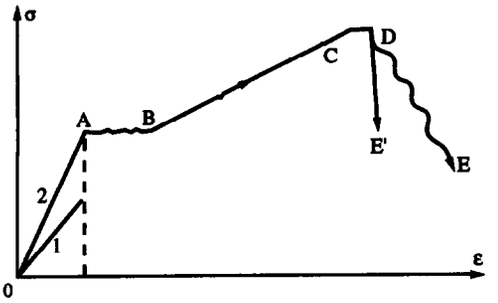

Fig. 1. Sketch of the tensile strength/strain trend for a bulk ceramic (curve 1) and a fibre-reinforced ceramic matrix composite (curve 2).

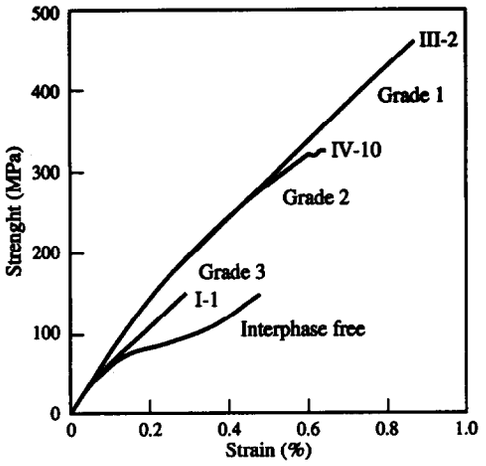

Fig. 2. Strength/strain behaviors for experimental C/C/SiC composites from the various grades and a C/SiC (interphase-free) composite.

which have to be kept confidential. They are built from about ten 2D carbon clothes (polyacrilonitrile-based fibres) which are stacked, then coated with a pyrolytic carbon interphase (from CVD) the thickness of which may vary from 80 to 800 nm, then infiltrated with a polycrystalline and pure SiC matrix (from CVI). Also, interphase-free composites were studied. Three different makes of carbon fibre have been used, including T300 from Toray (fibre A). However, no basic differences were detected in the resulting composites, though differences were observed between fibres. Discrepancies in surface topology between fibre types and the peculiar textural features of the T300 fibre (accumulation of cylindrical pores close to the surface, ring-like change in texture from isotropic to radial) were reported elsewhere from a TEM study.[2,3] As far as ultimate tensile strength, σ, and strain, ε, values coarsly evolve together (Table 1), the whole sample set (23 interphase-containing composites) is arbitrarily divided into three mechanical grades following a classification factor $F = \sigma \times \varepsilon$. Thus, composites from Grade 1 have $F > 350$, Grade 2 composites have $100 < F < 350$, and Grade 3 composites have $F < 100$. On the contrary, no relationships may be found between the grades and the interphase thickness. Tensile tests were performed by SEP according to their standard procedure (gauge length = 100 mm).

Textural and structural investigations have used a glass lens (macroscopic scale), a scanning electron microscope (SEM, micrometric scale) and a high resolution transmission electron microscope

Table 1. Description and three-grade classification of the sample set

	Code	*Fibre*	σ *(MPa)*	ε *(%)*	*Thickness (μm)*	*E (GPa)*	*F*
Grade 1	I—2	A	520	0·99	0·50	104	515
	II—1	A	450	1·00	0·30	82	450
	II—3	C	440	1·00	0·30	105	440
	V—6	A	430	0·96	0·30	89	413
	III—2	A	460	0·86	0·65	90	396
Grade 2	II—2	A	380	0·89	0·15	105	338
	II—4	C	410	0·84	0·15	88	344
	II—6	B	370	0·84	0·70	70	311
	III—1	A	400	0·86	0·40	88	344
	III—3	A	400	0·78	0·55	90	312
	III—4	A	400	0·78	0·50	85	312
	III—6	A	400	0·80	0·35	95	320
	III—7	A	250	0·50	0·80	75	125
	III—8	A	420	0·70	0·55	90	294
	IV—10	A	340	0·68	0·85	100	231
	V—1	A	240	0·49	0·50	91	118
	V—2	A	400	0·78	0·50	88	312
	V—3	A	310	0·57	0·60	76	177
	V—4	A	290	0·67	0·25	95	194
	V—5	A	360	0·74	0·25	92	266
Grade 3	I—1	A	150	0·31	0·50	76	47
	II—5	B	170	0·46	0·10	88	78
	III—5	A	140	0·18	0·08	130	25
Interphase—free	IV—12	A	160	0·50	—	133	—
	IV—13	A	120	0·25	—	80	—

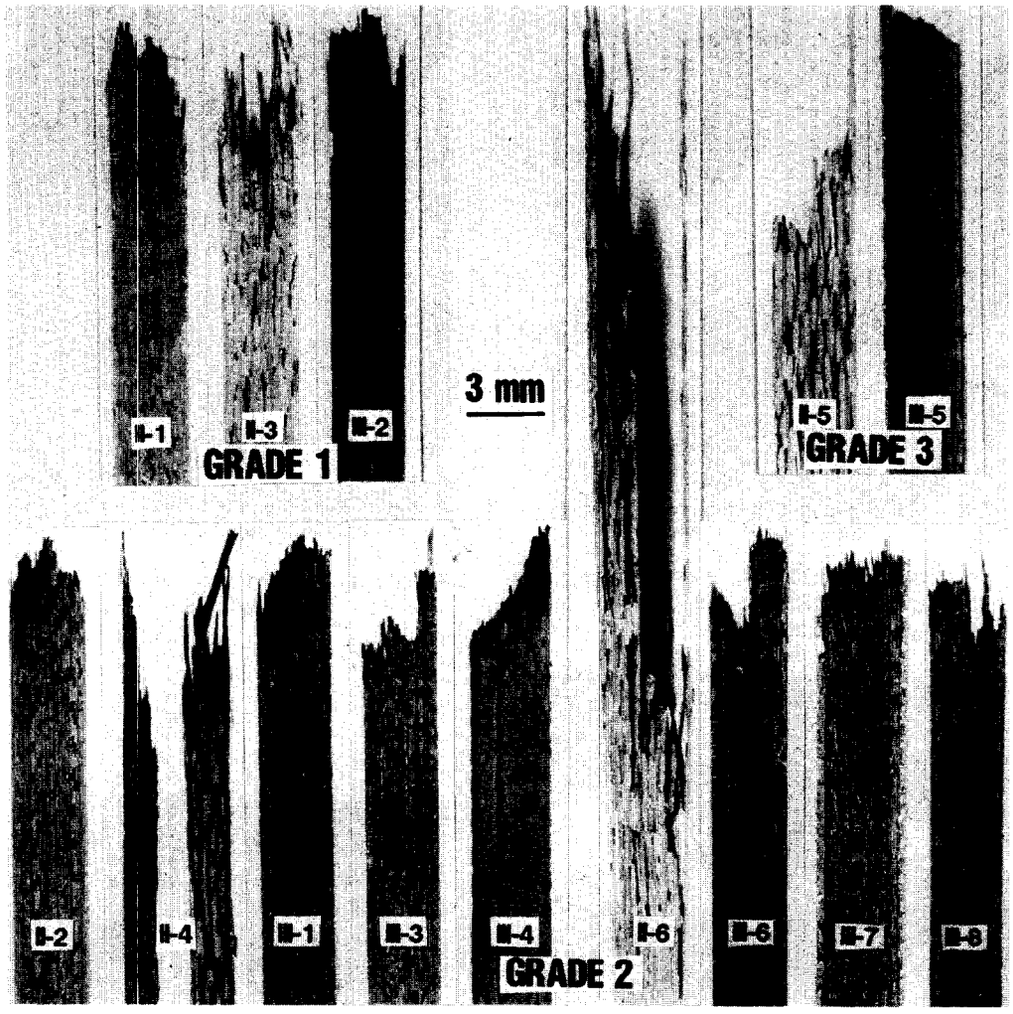

Fig. 3. Macroscopic fracture profiles of some composite samples from Grades 1, 2 and 3 (tensile test).

(TEM, nanoscopic scale). Only composite samples broken by the tensile test were examined by the glass lens and SEM (which required a Au coating to prevent charge effects). For TEM examinations, samples were taken from composites using diamond drilling performed far from the damaged zone, then prepared using a diamond saw into 3 mm disks, which were mechanically thinned (diamond powder polishing) then ion-thinned with argon ions (Gatan DUOMILL and IONTECH). TEM microscopes were Philips CM12 and Philips EM400 (120 kV). Contrasted bright field (BF), dark field (DF), lattice fringes (LF) and selected area diffraction (SAD) modes were used following conventional procedures; DF was more specifically[4] used for imaging carbon. Regarding the micrographs, DF images are mainly obtained from the 002 reflection of polyaromatic turbostratic carbon. Any graphene stack (graphene = a single polyaromatic layer) not disposed edge-on relative to the electron beam (i.e. not disposed perpendicularly to the plane of the picture) will therefore not be imaged. Because of the use of a small objective aperture, the DF images are built only with a small length of the 002 ring and therefore provide directional information. Taking two successive pictures using two orthogonal positions for the objective aperture helps any possible anisotropy to be revealed. If the two pictures appear statistically identical, (similar number and size of bright domains) the carbon material is isotropic (zone 1 in Fig. 11 for instance). If they are not, the carbon material is anisotropic (zone 2 in Fig. 11 for instance). The mean azimutal orientation is shown by the '=' sign on each picture.

Optical diffraction using a laser source has also been performed on original LF micrograph films, when lattice fringes were imaged. The diffraction patterns thus obtained act as a very local electron diffraction (scattering area is about 600 nm^2).

3 Results

3.1 Macroscopic scale

The tensile test samples were examined after mechanical testing, in order to tentatively reveal any possible correlation between the fracture profile and the mechanical behavior observed. Figure 3 illustrates the fracture profiles of the tensile test

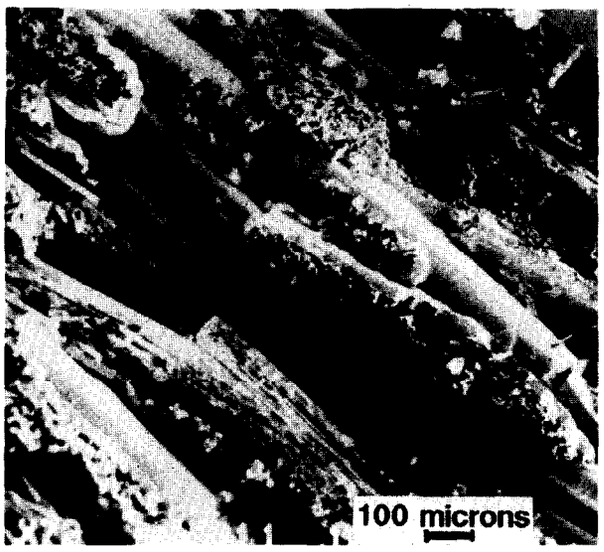

Fig. 4. Characteristic enlarged SEM view of tows within any C/C/SiC composites. Tows may often be considered as independent entities.

Fig. 5. Example of the mechanical independence of neighboring tows: one is fractured, while the transverse one is not (SEM view).

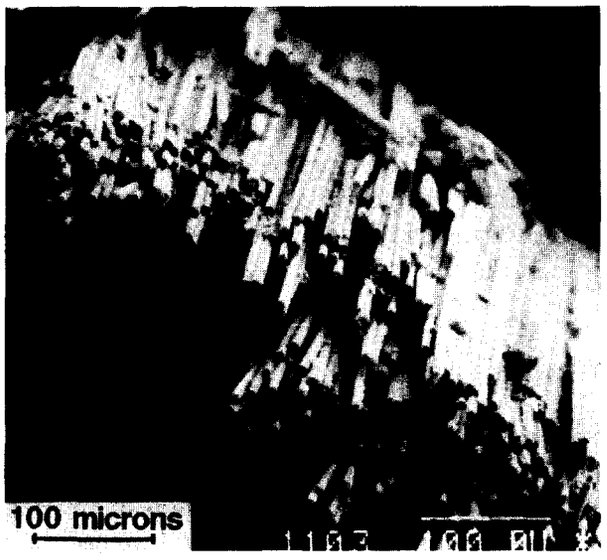

Fig. 6. Typical SEM view of the fracture surface of a tow within a Grade 1 composite.

Fig. 7. Typical SEM view of the fracture surface of a tow within a Grade 3 composite.

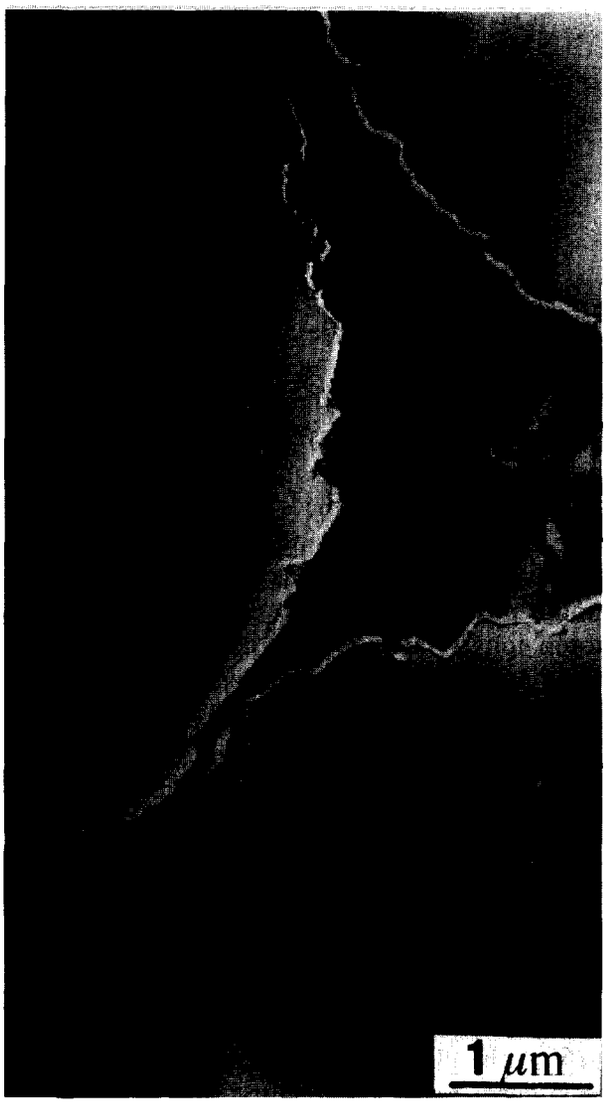

Fig. 8. Low magnification BF TEM view of a decohesion path in an interphase-free composite (C/SiC).

samples of some composites from Grades 1, 2, or 3. Obviously, a specific grade is not characterized by a specific fracture profile. For instance, samples II-5 and III-5, though both from Grade 3, exhibit very different fracture profiles. The profile amplitude is about 10 mm for the former, while only 2 mm for the latter. Likewise, samples II-6 and III-1 from Grade 2 have fracture profile amplitudes of 30 and 3 mm respectively. Therefore, no simple relationship exists between the fracture profile and the ultimate tensile strength value of the C/C/SiC composites.

3.2 Microscopic scale

A general statement is that all the C/C/SiC composites are built from an elementary entity, which is defined as a tow of pyrocarbon-coated carbon fibres, covered with a silicon carbide sheath which is more or less able to densify the tow (Fig. 4). This suggests that tows should be independent of one another regarding failure propagation, as illustrated in Fig. 5 which shows that a longitudinal entity has been damaged, while the neighboring transversal entity has not.

Starting from the statement above, simple correlations are now able to be found between the fracture profiles and the various grades, when considering the tows as 'basic mechanical units'. Indeed, any Grade 1 composite was found to mainly contain tows exhibiting fibre pull-out at the fracture surface (Fig. 6), while any Grade 3 composite was found to mainly contain tows exhibiting an almost planar fracture surface (Fig. 7). Therefore, the fracture profiles of the tows, rather than the fracture profiles of the composites, are related to the macroscopic mechanical features of the C/C/SiC composites. Obviously, this must be governed by the behavior of the pyrolytic carbon interphase within the tows.

3.3 Microscopic and nanoscopic scale

Prior to describing the pyrocarbon-containing composites, Figs 8 and 9 illustrate some specific features of the pyrocarbon-free composites. Firstly, decohesions at the fibre/matrix interface

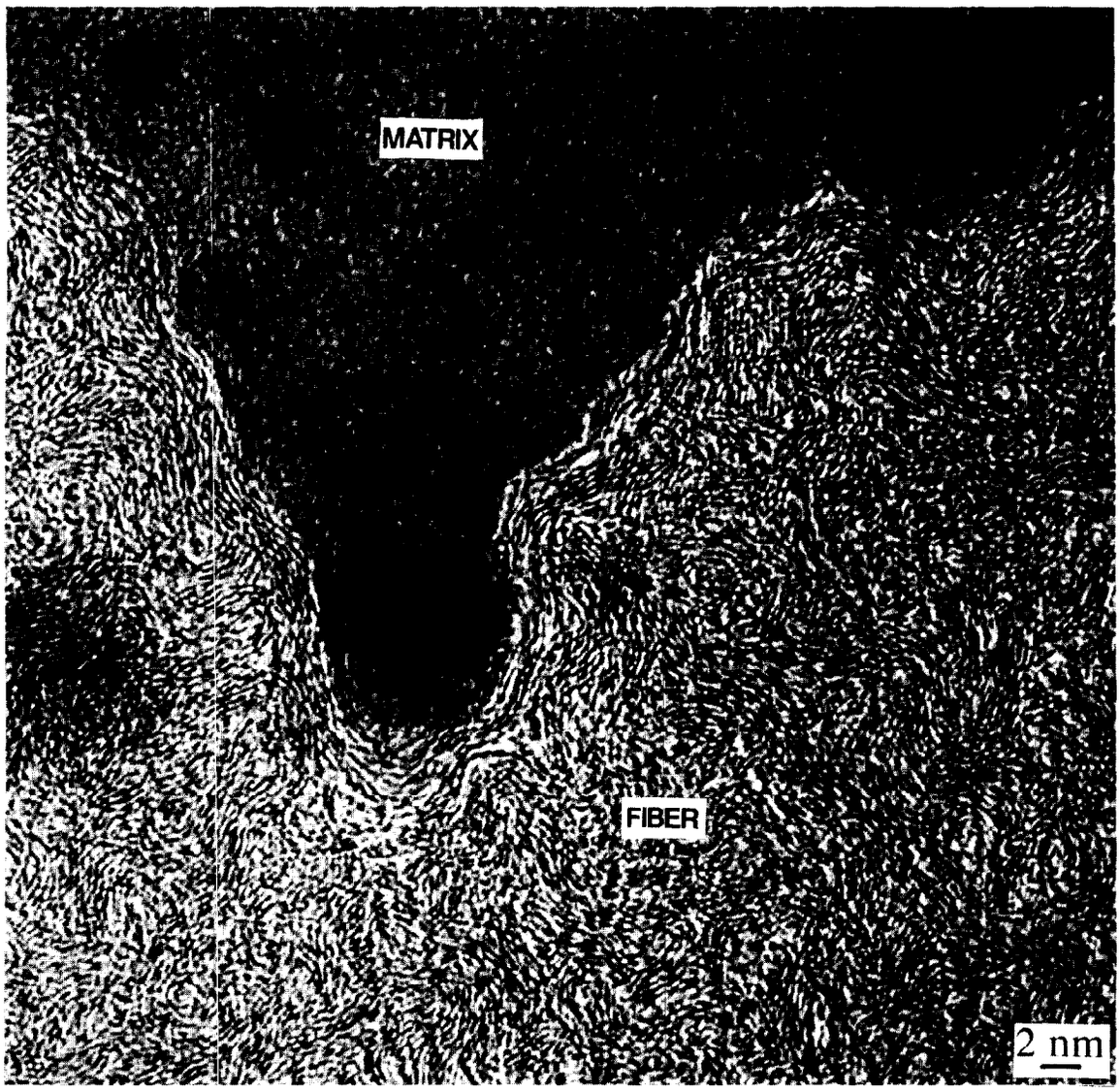

Fig. 9. LF TEM image of the fibre/matrix interface in an interphase-free composite (C/SiC).

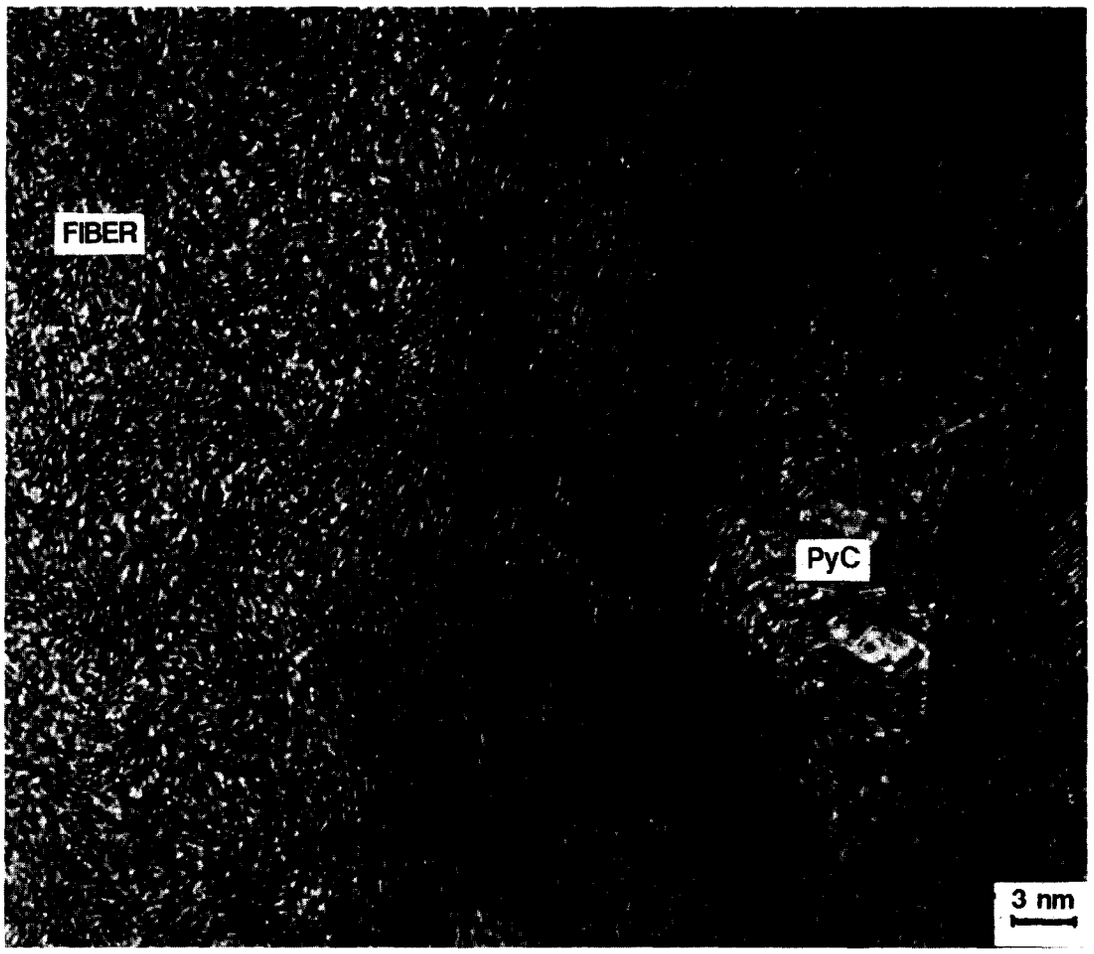

Fig. 10. LF TEM image showing how the fibre surface induces a local anisotropy of the graphene stacks at the very beginning of the pyrolytic carbon deposition.

are systematic (Fig.8), indicating that no chemical interactions occur between the carbon of the fibre and the SiC crystals. Because no pyrocarbon is covering the fibre surface, the texture of the graphene stacks at the fibre surface is clearly observable (Fig. 9). Obviously, the last 3–5 graphene layers are oriented parallel to the fibre surface (T300 fibres in that case). Such a texture does not help in promoting chemical reactions between polyaromatic carbon and SiC. Decohesions are certainly due to the difference in thermal expansion coefficients (TEC), i.e. 15–20 $\times$ 10^{-6}/K for the fibre transversally, and 4 $\times$ 10^{-6}/K for the SiC matrix, rather than to the mechanical test, and therefore are an intrinsic feature of the composites. However, because of the lack in adhesion between the fibre and the matrix, the multiple fracture of the matrix is probably not directly due to the difference in TEC but to the anisotropic stresses induced by the presence of the reinforcement during the shrinkage of the matrix when cooling. Figure 9 also illustrates the depth of the roughness of the fibre (T300) surface, which can reach about 25% of the fibre diameter for the T300, while only about 3% and 10% for fibres B and C respectively.

Investigating all the samples using TEM has allowed three interfacial pyrocarbon texture types to be described. Whatever the texture type or the grade for the C/C/SiC composites, the first ten nanometers of the pyrolytic carbon are deeply influenced by the fibre topology (Fig. 10). Graphene stacks are highly anisotropic and lie flat upon the fibre surface, despite its rather high roughness.

3.3.1 Bimorphic interphases

These are made of two parts of equal thicknesses. The pyrolytic carbon texture of the fibre-side part is identified as 'bulky oriented isotropic' (BOI-PyC), i.e. all the possible orientations are found for the graphene stacks which the pyrocarbon is made of, but a main specific orientation—parallel to the interfaces—is found (Fig. 11, zone 1). The pyrolytic carbon texture of the matrix-side part is described as 'anisotropic' (ANI-PyC), since no graphene stacks oriented perpendicularly to the main direction of orientation—again parallel to the interfaces—are found (Fig. 11, zone 2). At high magnifications (LF mode), the change in texture from zone 1 (BOI-PyC) to zone 2 (ANI-PyC) appears progressive (Fig. 12). The related optical

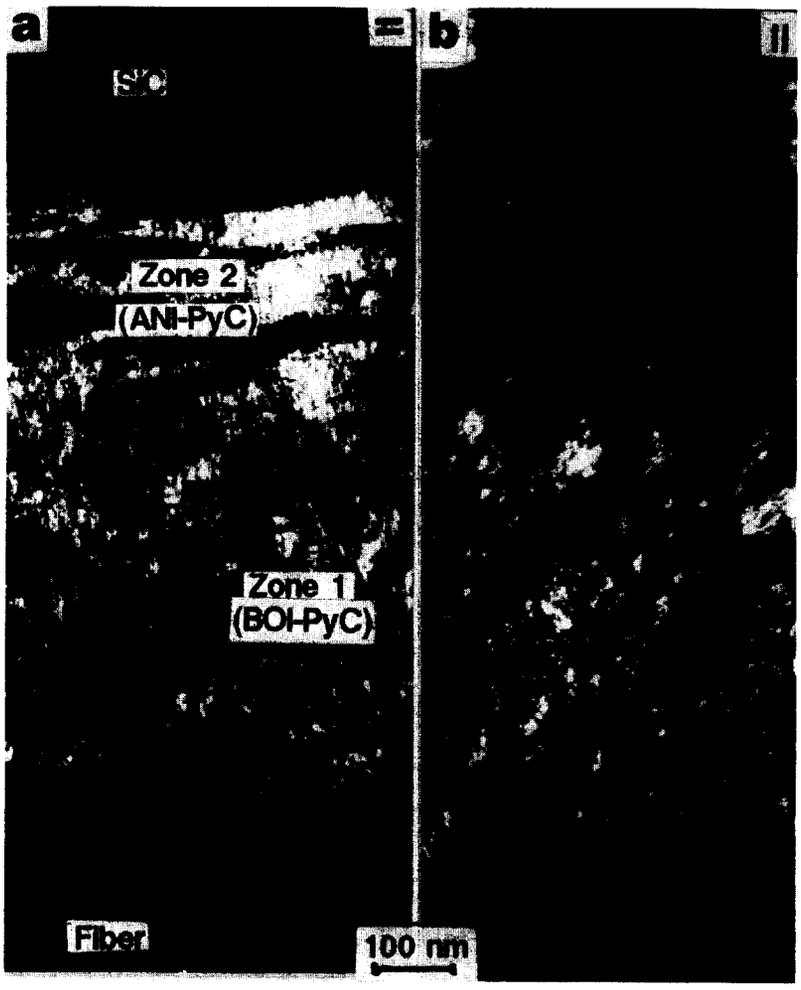

Fig. 11. C_{002} DF micrographs of a bimorphic-type interphase: two orthogonal orientations are imaged. (a) The two parts (zones 1 and 2) of the pyrocarbon interphase appear very bright. (b) Zone 1 is still lighted-on but does not appear bright, while zone 2 appears dark. Zone 1 therefore corresponds to a bulky oriented isotropic carbon (BOI-PyC) and zone 2 corresponds to an anisotropic carbon (ANI-PyC).

diffraction patterns in Fig. 12 well illustrate how the anisotropy increases from the fibre side (bottom) to the matrix side (top). The 002 ring is progressively replaced by two 002 arcs, the angular opening of which decreases as the extent of angular misorientations between graphene stacks decreases, and therefore becomes smaller. Close to the matrix (Fig. 13), the graphene stacks are very well organised, inducing a high anisotropy and a specific contrast effect as dark bands (so-called Bragg fringes) perpendicular to the direction of carbon layers.

Within the ANI-PyC texture (zone 2), slit pores are often observed, actually indicating a lenticular porosity, as far as the transverse or longitudinal views of the interphase are identical. Pore walls are made of sheets of graphene stacks locally disconnected (Fig. 14). Lateral transitions from area of high compactness to area with lenticular porosity are rather sudden, and nearly periodic (Fig. 15).

Within the bimorphic interphase type, decohesions always occur either at the pyrocarbon/matrix interface, or at the zone 1/zone 2 transition or within the ANI-PyC (Fig. 16). Obviously, the anisotropic but entangled texture is efficient in dispersing the fracture energy through a multiple fracture effect.

3.3.2 Carbon wall-ending interphases

The main part of the interphase is from the BOI-PyC type, previously described. It corresponds to the light-on part in Fig. 17(a). However, the very end part of the carbon interphase (i.e. matrix side) is made of a different texture, specifically long carbon walls preferentially oriented perpendicularly to the interfaces. They are shown in Fig. 17(b). The carbon wall zone is highly porous as seen in Fig. 18, which also illustrates the perfection of the graphene layers within the walls since they exhibit Bragg fringes, which indicate their high organisation. Important features are that the walls penetrate deeply within the SiC matrix (Figs 17(b) and 19), sometimes as far as 100 nm. The end tip of the carbon walls may exhibit an edge shape which enhances the possibility of chemical bonding with the surrounding SiC crystals (Fig. 19).

Within the carbon wall-ending interphases, decohesions are always observed at the BOI-PyC/fibre interface, or within the BOI-PyC (Fig. 20).

3.3.3 Mixed interphases

These exhibit textures combining features of both interphases. Thus, the whole pyrocarbon texture may be a mere BOI-PyC texture without being associ-

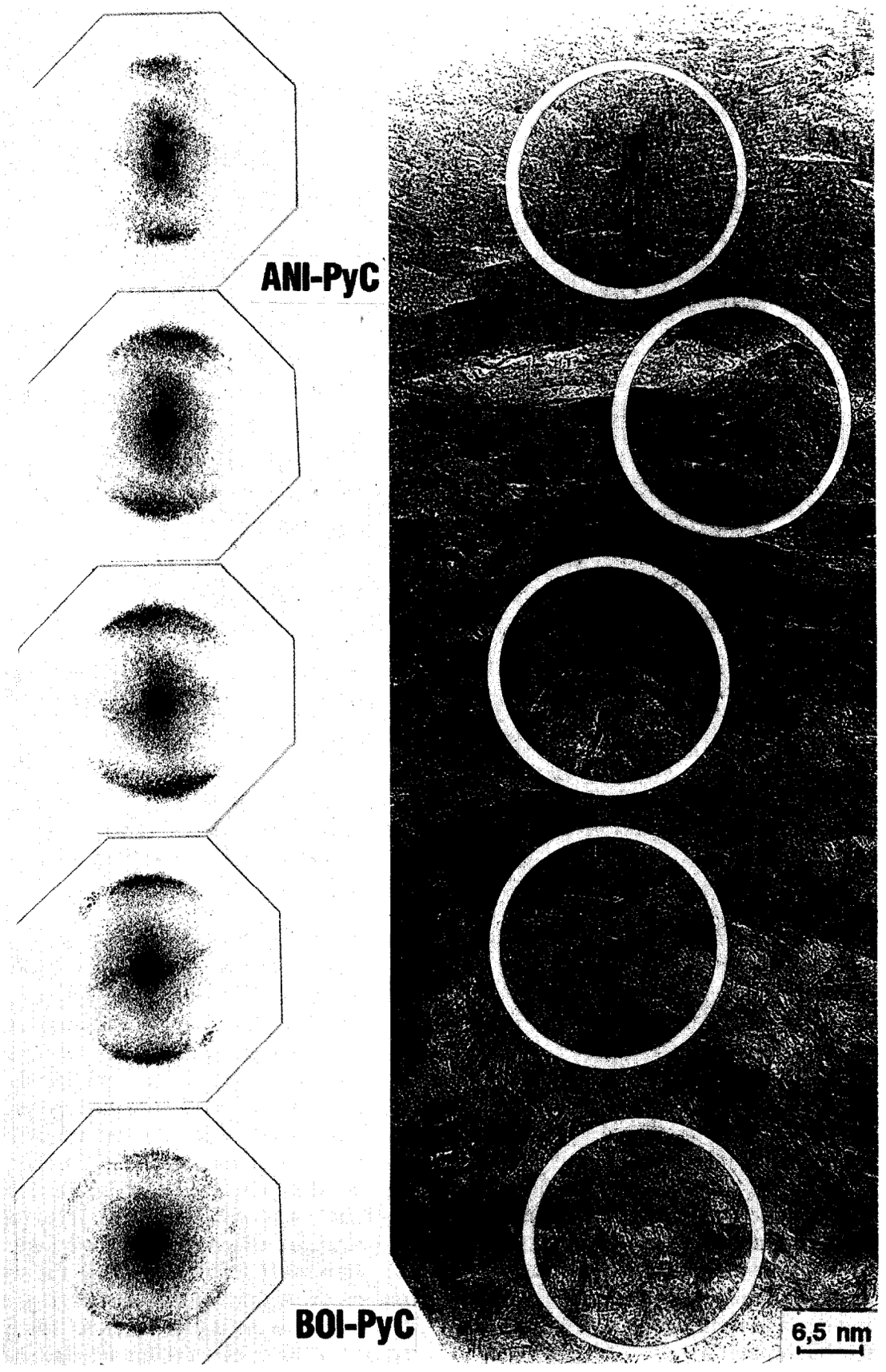

Fig. 12. LF TEM images of the zone 1/zone 2 transition within a bimorphic texture pyrocarbon interphase. Related optical diffraction patterns are inserted. Fibre side is below, matrix side is above.

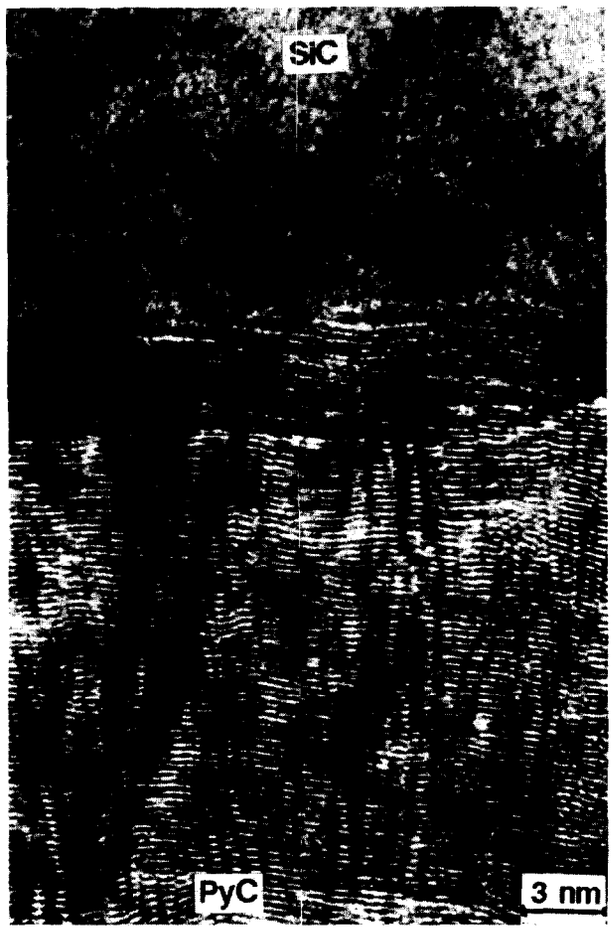

Fig. 13. LF TEM image of the pyrolytic carbon interphase (ANI-PyC) matrix interface. Note the high anisotropy parallel to the interface, and the nearly perfect organisation of the graphene sheets.

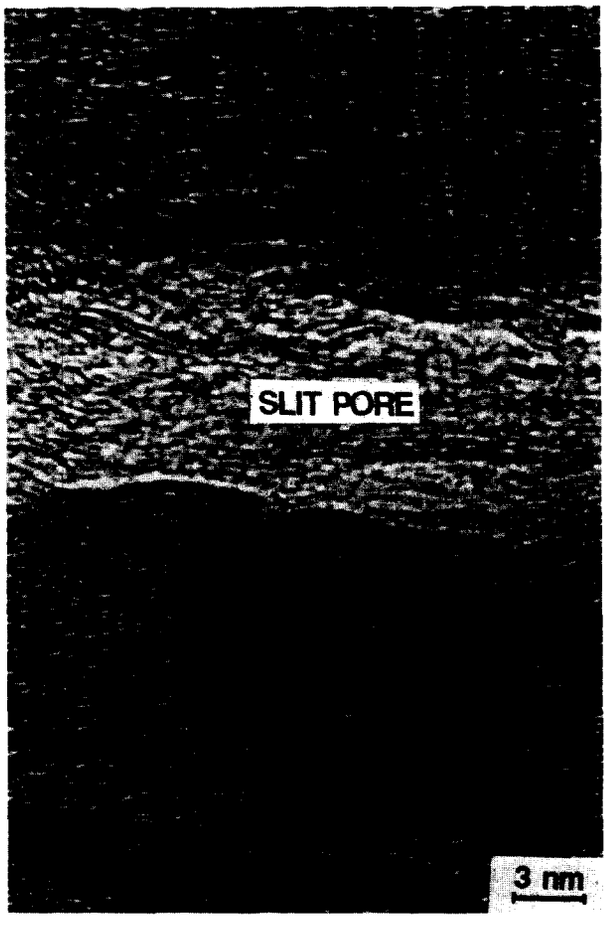

Fig. 14. LF TEM image of a slit (lenticular) pore within the ANI-PYC part of the interphase. The contrast within the pore is due to overlapping matter.

ated with any carbon-wall or ANI-PyC texture (Fig. 21, right), or may also be similar to a bimorphic type including a ANI-PyC part—but with a lower anisotropy (Fig. 21, upper left, Fig. 22). Anisotropic textures may be associated with graphene layers penetrating the SiC matrix and therefore resembling a carbon wall-ending interphase (Fig. 22).

4 Discussion

There is an exact correspondence between the three texture types of the pyrocarbon interphase described above and the three composite grades as defined in Section 2. Specifically, all the Grade 1 composites exhibit bimorphic pyrocarbon interphases. Grade 3 composites exhibit carbon wall-ending pyrocarbon interphases, and Grade 2 composites contain mixed interphases.[5] Considering the latter grade, it is worthy to note that interfacial areas may have different textures, though very close to each other (Fig. 21). On the contrary, Grades 1 and 3 are homogeneous.

Therefore, textural discrepancies in the interphases may originate from differences in deposition conditions. In addition to differences in the process, differences may also be very local, as shown by the interphase heterogeneities found in Grade 2 composites. This was rather expected, because of the 3D porous feature of the preform which is likely to induce local differences in gas flows, partial pressures, turbulences, etc. On the other hand, regarding the effect expected from a porous substrate, the interphase homogeneity of Grade 1 or 3 composites is remarkable.

4.1 Bonding strength of the various interfaces

Considering all the interface types encountered and the location of the decohesion paths in the composites (whatever the grade) allows the various interfaces to be ordered following the increasing bonding strength (Table 2). Actually, decohesions, due to either the tensile test or the preparation method for TEM examination, indicate the weak interfaces within the composites. Obviously, the weakest interface is the fibre/matrix interface in the pyrocarbon-free composite.

The ANI-PyC/matrix interface in Grade 1 composite is stronger but still weak, since no chemical bonding other than weak interactions are allowed by the planar (polyaromatic) faces of graphene

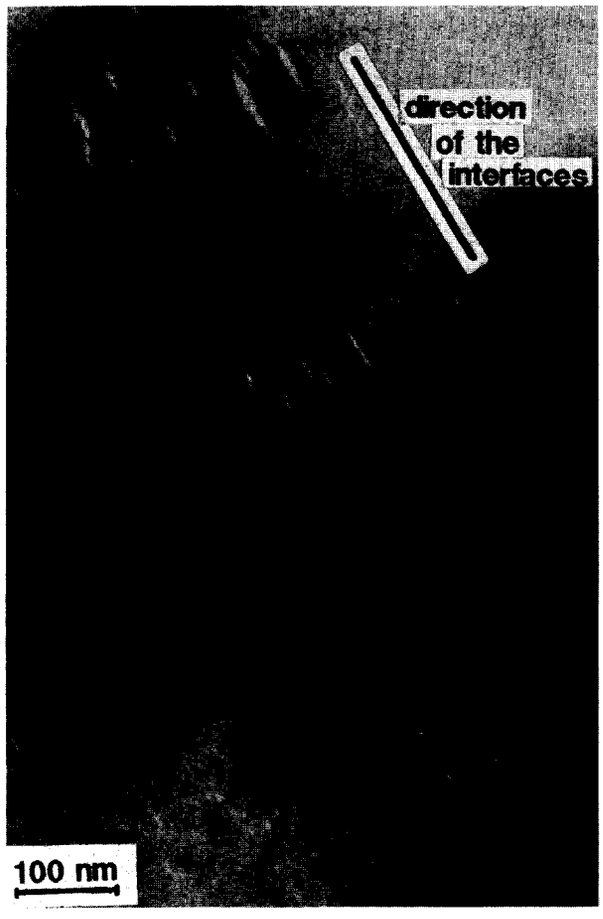

Fig. 15. BF TEM image of a carbon interphase exhibiting a nearly periodic occurrence of the lenticular porosity.

sheets. It could be wondered why the interface always exhibits a PyC/matrix contact (except when disturbed by a failure due to the mechanical test) instead of showing the same voids due to TEC differences, as in the pyrocarbon-free composite. This is probably due to a compensation effect of the pyrocarbon interphase, which is related to the presence of the lenticular porosity in the ANI-PyC part, and which will be discussed later.

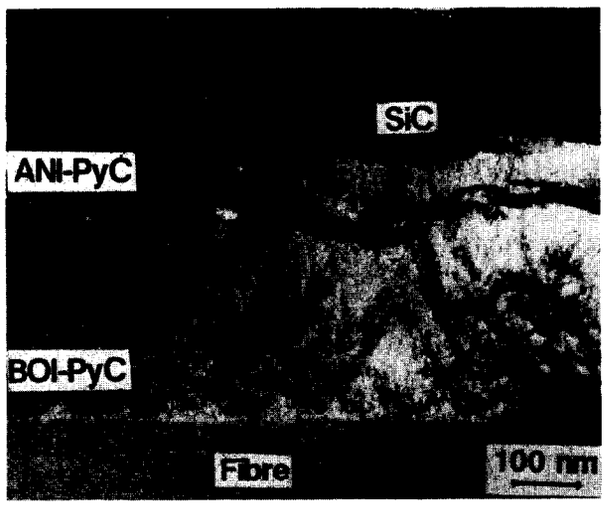

Fig. 16. Low magnification C_{002} DF image of a decohesion path within a bimorphic-type pyrocarbon interphase.

Table 2. Classification of the various interfaces in order of decreasing bonding strength

Interface	*Grade*	*Bond*
PYCX/matrix	3	σ chemical bond
Fibre/PyC	All	A majority of σ, and Van der Waals
PyC/matrix	2	Van der Waals and σ
BOI-PyC/ANI-PyC	1	Van der Waals and σ
PyC/matrix	1	Van der Waals
Fibre/matrix	Free	'Mechanical' bond

However, placing this interface type before or after the BOI-PyC/ANI-PyC interface in Table 2 is difficult since it depends on the degree of mixity.

Certainly stronger is the BOI-PyC/ANI-PyC interface in Grade 1 composites, since it allows both Van der Waals bonds—when graphene sheets are arranged face to face—and chemical (covalent) bonds—when graphene sheets are arranged edge-to-edge, or through defect sites.

The BOI-PyC/matrix interface in Grade 2 composites is stronger than the ANI-PyC/matrix interface mentioned above since it enhances the possibility of covalent bonds.

Even stronger is the fibre/BOI-PyC interface in Grade 1, 2, or 3 composites, where one failure only has been observed among about 100 interfaces investigated. Proportions of covalent bonds are higher than with the BOI-PyC/ANI-PyC interface, though also dealing with graphene/graphene interactions. It is assumed that the proportion of potential sites for covalent bonds increases as the number of defects and grain boundaries increases, with respect to the mean size of the coherent domains (i.e. the length *La* of the straight carbon layers within associated graphene stacks). Actually, it is obvious that the sizes of the coherent domains are smaller for the carbon fibre (see Fig. 9 for instance, where *La* ~2 nm) than for the pyrolytic carbon deposit (see Fig. 10 for instance, where *La* = 3–5 nm for the BOI-PyC deposit, and Fig. 13 for instance, where *La* > 10 nm for the ANI-PyC deposit). In addition, the BOI-PyC/fibre interface, because of the fibre topology, is much rougher than the ANI-PyC/BOI-PyC interface, which is not likely to promote easy delamination. Therefore, both structural and textural considerations are able to explain the difference in strength between the two graphene/graphene interfaces.

Finally, the strongest interface is the PyC/matrix interface encountered in Grade 3 composites, which is characterized by carbon walls perpendicular to the interface and deeply inserted into the matrix. This originates from the fact that the carbon walls are strongly linked on the one hand to the pyrocarbon on the other hand to the SiC

crystals by σ bonds. The high strength of the aromatic C = C bonds (the highest for solids) of the nearly perfect graphenes which the carbon walls are made of prevents any strain or shearing to occur, either perpendicular or parallel to the interface.

4.2 Mechanical behavior of the composites related to their interfacial features

Considering Table 2 explains why Grade 3 composites have the strongest fibre/matrix bonding of the sample set. Indeed, they contain the two

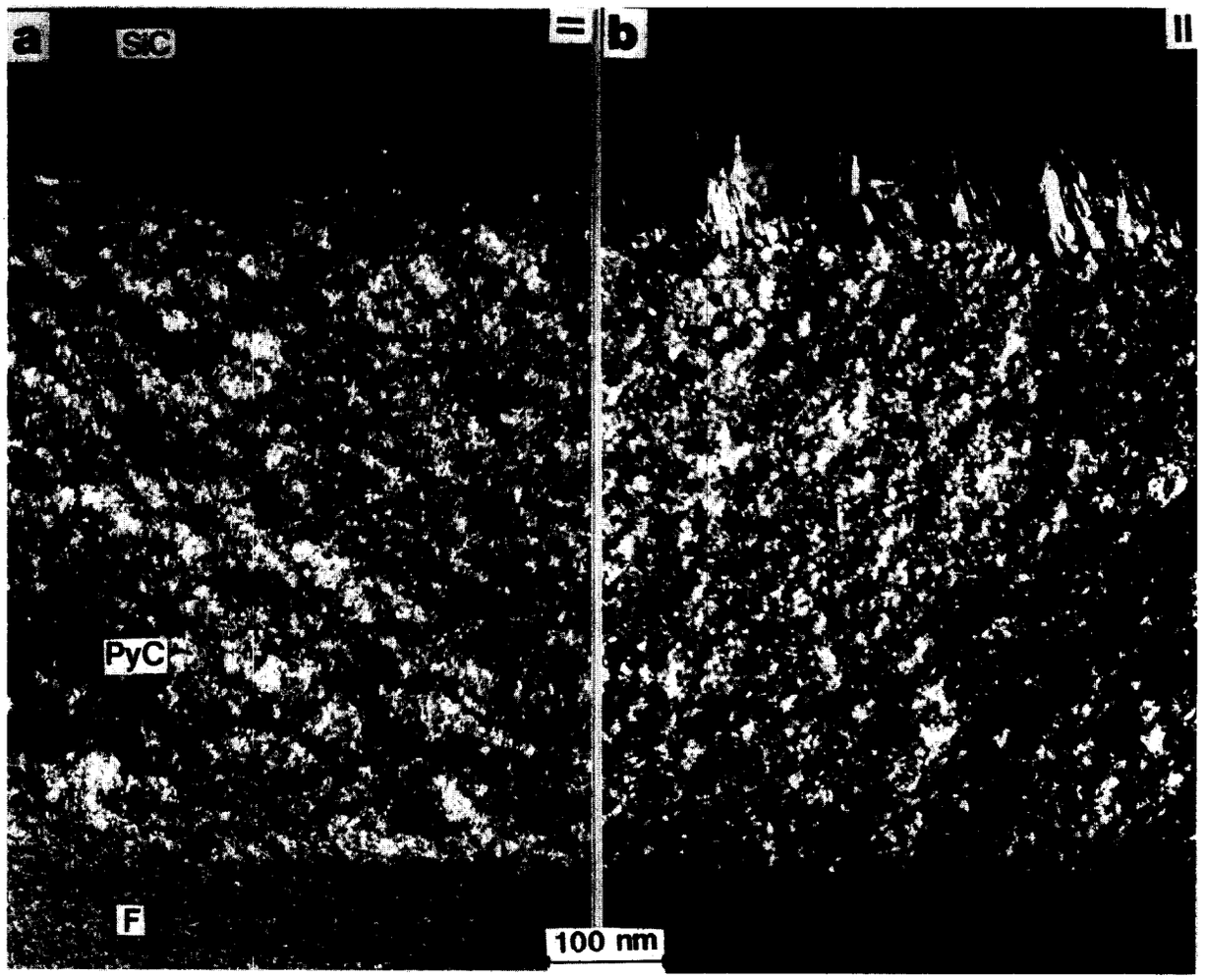

Fig. 17. Two orthogonal DF TEM images of a wall-ending type pyrocarbon interphase. Comparing (a) and (b) indicates that the whole pyrocarbon interphase is from the BOI- PyC type texture. Micrograph (b) clearly evidences the carbon walls (see text) as bright stripes oriented perpendicularly to the pyrocarbon/matrix interface.

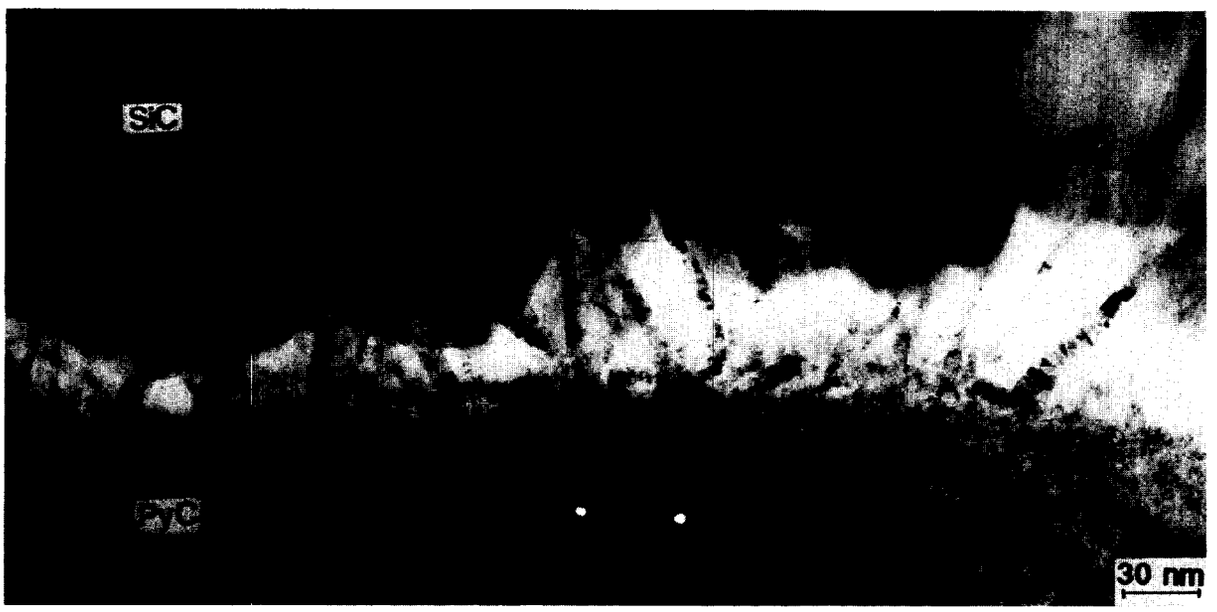

Fig. 18. BF TEM image of a carbon wall area. Note the high porosity.

strongest interfaces encountered. Therefore, a failure will progress straight from the matrix (which is the component with the lowest deformability) to the fibre through the interphase, in order to follow the strain induced by the opening of the failure edges (Fig. 23(a)). At the other extreme, Grade 1 composites have two weak interfaces, in which the

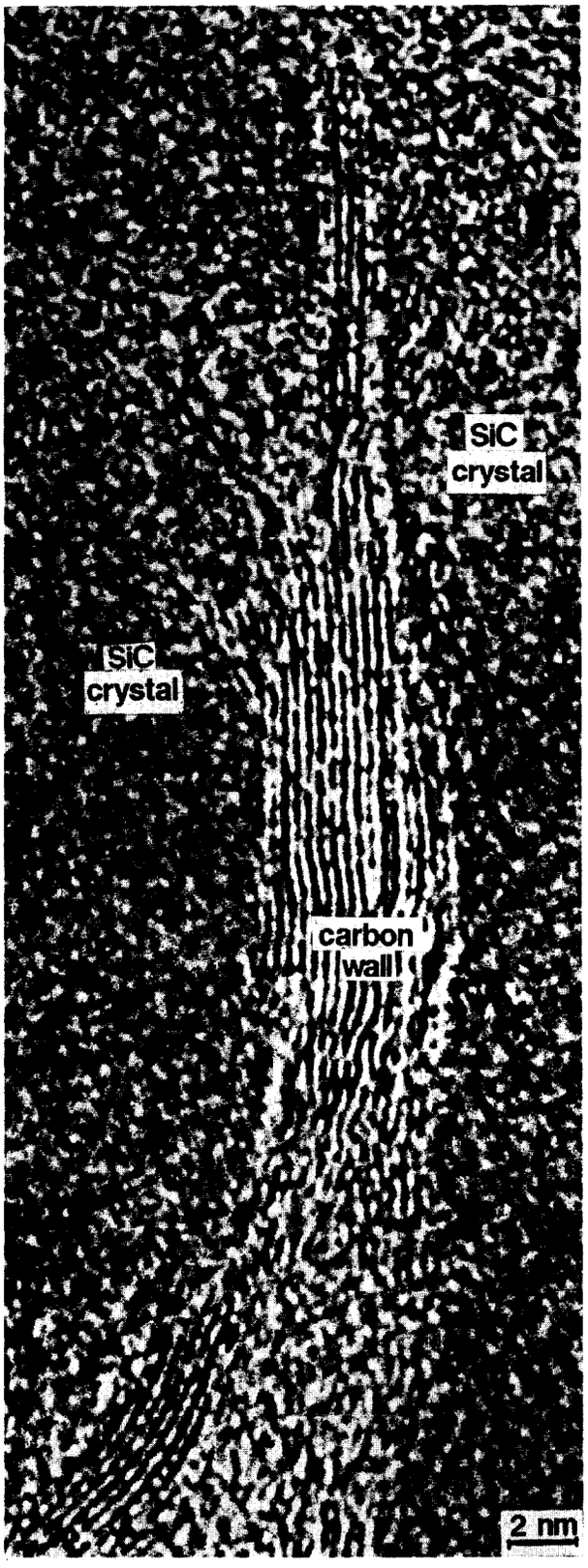

Fig. 19. LF TEM image of the end tip of a carbon wall between SiC crystals, exhibiting a peculiar edge-shape.

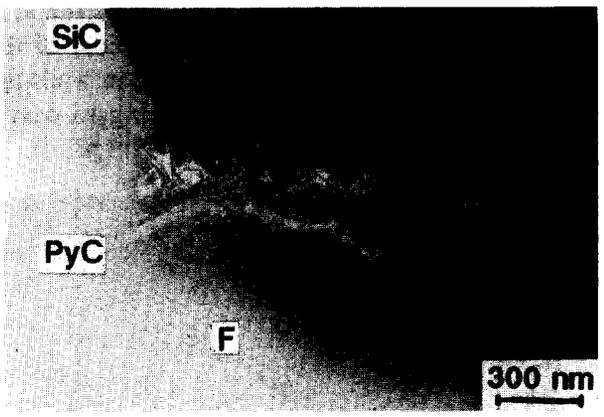

Fig. 20. Low magnification BF TEM view of a decohesion path within a carbon wall-ending type pyrocarbon interphase.

ANI-PyC part of the interphase is involved. Because the ANI-PyC is able to easily delaminate due to the anisotropic orientation of graphenes, the strain which goes with the crack propagation will not concern the fibre since it is somewhat compensated by a mode I/mode II change of the failure path (Fig. 23(b)). Successive delaminations within the ANI-PyC will help the fracture energy to disperse, and are likely to restrain the failure propagation until possibly stopping it. The fibre rupture will thus be delayed, leading to the highest ultimate strength values. Describing such an interphase as a 'fuse' is common but not appropriate, as far as the 'fuse' concept would mean that the interphase would not play any role in the mechanical behavior of the composite but once, i.e. until a critical value for the applied strength is reached

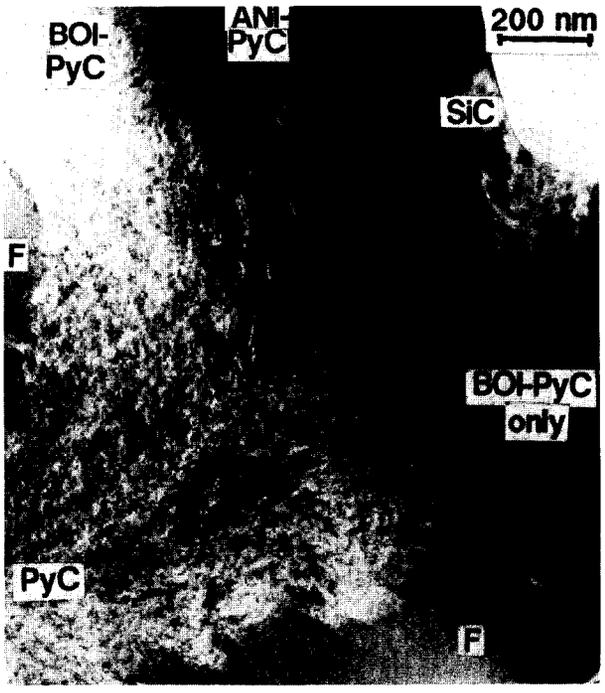

Fig. 21. BF TEM view of an example of mixed type associated interphases.

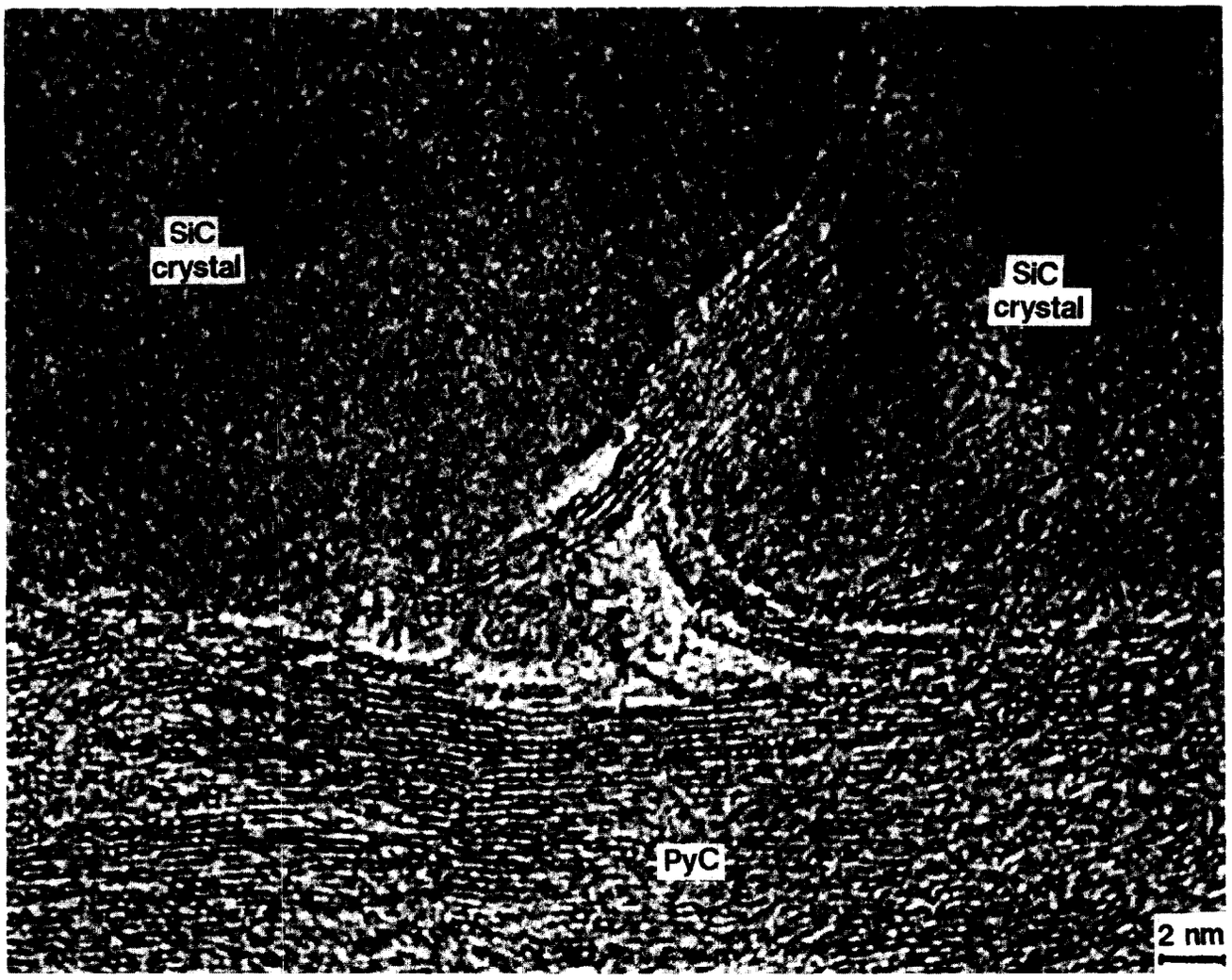

Fig. 22. LF TEM image of an example of a mixed type interphase. Note the combination of a ANI-PyC type texture with a carbon wall-ending type texture.

(corresponding to the fusing current for the electrical fuse). Obviously, the role of the interphase is not that binary, since helping in preventing the failure far before the ultimate strength is reached.

These considerations are consistent with the observations that tows exhibit mirror type fracture profiles in Grade 3 composites, while they do not exhibit planar fracture profiles in Grade 1 composites.

Due to the intermediate features of their interphases, Grade 2 composites logically behave intermediately, combining the two extreme fracture mechanisms described above in various proportions.

Finally, Table 2 indicates that the interphase-free composite has the weakest interface (PyC/fibre interface). Because differences in CET induce an interfacial void, the interface is too weak to allow the fracture energy to disperse. Even though the mode I failure propagation will again change for a mode II, the energy is fully maintained and the stress is quickly transferred to the fibre. However, the fibre will not break in front of the failure exit site within the matrix, but somewhere else along the fibre where strength is weakened by defects.

4.3 Origin of the carbon walls

Carbon walls, lying perpendicular to the interface at the pyrocarbon/matrix transition, are mainly observed in Grade 3 composites. Because they have been already observed in pyrocarbon-free SiC/SiC composites,[6–8] they have to be considered as an early step phenomenon of the SiC matrix deposition process, rather than a late step phenomenon of the pyrocarbon deposition process. They have been previously assumed to originate from the transformation of SiC crystals into C (and SiO_2, because of the presence of oxygen traces),[6] or to the decomposition into Si species and solid C of the early SiC crystals which could be abnormally unstable.[7,8] Indeed, some time is certainly required for the CVI process parameters to reach the steady-state, inducing transient and inappropriate turbulences, gas proportions, etc.[7,8] Both hypotheses are complementary, and oxygen

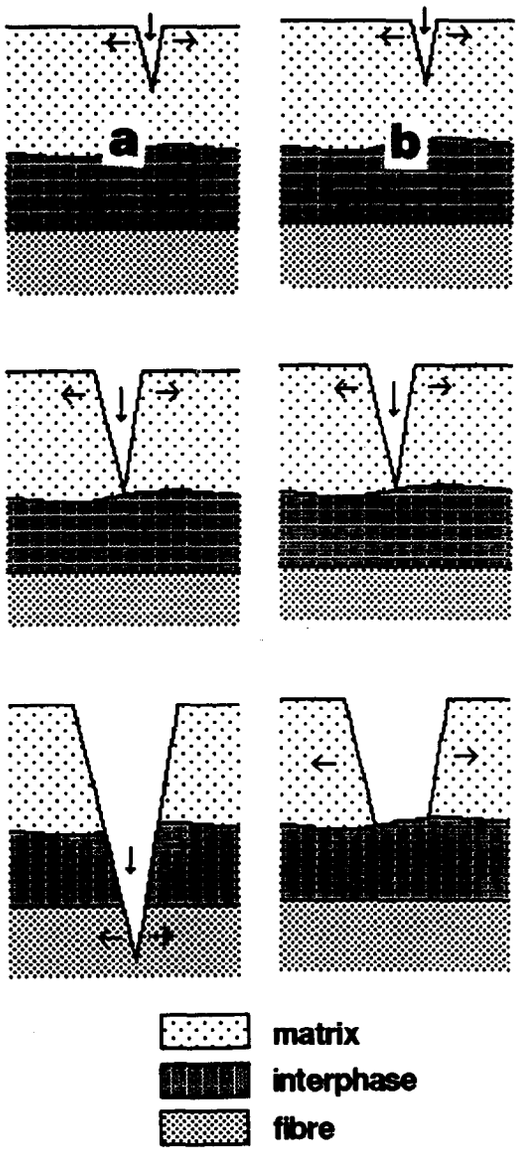

Fig. 23. Sketches of failure propagation: (a) Grade 3 composites; (b) Grade 1 composites.

traces present at the early step of the CVI process are likely to combine quickly with Si to form gaseous SiO. No silica was observed in our composites, nor those of Refs 7 and 8, but SiO_2 may be reduced to gaseous SiO as soon as gaseous hydrocarbons or hydrogen are present. Actually, such gases are used in the CVI process. Also, the presence of oxygen traces and hydrocarbons may possibly promote the direct transformations of SiC into gaseous SiO, SiH_4, SiH and solid C.[9]

4.4 Lenticular porosity

Grade 1 composites often exhibit a lenticular porosity, located within the ANI-PyC part of the bimorphic interphase. The texture suggests local decohesions between graphenes, favored by the weakness of the graphene/graphene interactions (when parallel). Such decohesions do not seem to occur spontaneously in anisotropic pyrolytic carbon films when deposited on polished alumina plates at least in the 1050–1200°C temperature range.[3,10] Therefore, we assume that they are again due to differences in TEC. Actually, the TEC for the fibre is about 20×10^{-6}/K in a transverse direction, since it is statistically isotropic. This is rather high as compared with the TEC value in the direction of the graphene sheets, which is similar to that of graphite, when considered parallel to the graphene direction (no expansion). Likewise, the TEC on the ANI-PyC part of the pyrocarbon interphase in a direction perpendicular to the graphene sheets is close to that of graphite ($28{\cdot}5 \times 10^{-6}$/K). On the opposite, the TEC for the SiC matrix is rather low (4×10^{-6}/K). Taking into account on the one hand the various TEC values above for the various phases within a Grade 1 composite, and considering on the other hand the fact that the occurrence of the lenticular porosity has appeared to be somewhat periodic, simple calculations below have allowed the lenticular porosity to be simulated (Fig. 24). The calculations mean that, while the SiC matrix does not shrink much during cooling, the fibre shrinks a lot, relatively. Because the pyrocarbon interphase is firmly bonded to the fibre, the interphase has to follow the fibre shrinkage. However, because of the low TEC along the graphene sheets, the circumference of the ANI-PyC part of the interphase all around the fibre remains unchanged. Therefore, the ANI-PyC part is led to wrinkle, that induces internal stresses strong enough to overcome the weak Van der Waals bonds between graphene and to promote decohesions (lenticular porosity).

Considering a carbon fibre 7 μm in diameter, coated with a thin pyrolytic carbon layer (thin enough for its thickness being neglected relative to the fibre diameter) partly having a ANI-PyC texture, then surrounded with a SiC matrix, both submitted to a 1000°C difference in temperature from the preparation conditions to ambient. The 'length' L_0 of the ANI-PyC around the fibre is taken equal to the circumference C_0 of the fibre and is $7 \times \pi = 22$ μm. The shrinkage of the fibre diameter during cooling is $7 \times 20 \times 10^{-6} \times 1000 = 0{\cdot}14$ μm. The circumference C imposed to the ANI-PyC by the fibre shrinkage is then $21{\cdot}56$ μm, while the real length L of the ANI-PyC remains 22 μm ($L = L_0 = C_0$). Considering a period of ~0·2 μm between the occurrence of slit pores (see Section 3 and Fig. 15), there are $21{\cdot}56/0{\cdot}2 = 107{\cdot}8$ periods around the fibre. The length x of the triangular unit of the slit pores (Fig. 24) is thus $22/(2 \times 107{\cdot}8) = 0{\cdot}102$ μm. This allows the height h of the pore to be calculated at $h \sim 20$ nm using trigonometry.

Although the calculations above are simple—even simplistic—they indicate that the porosity

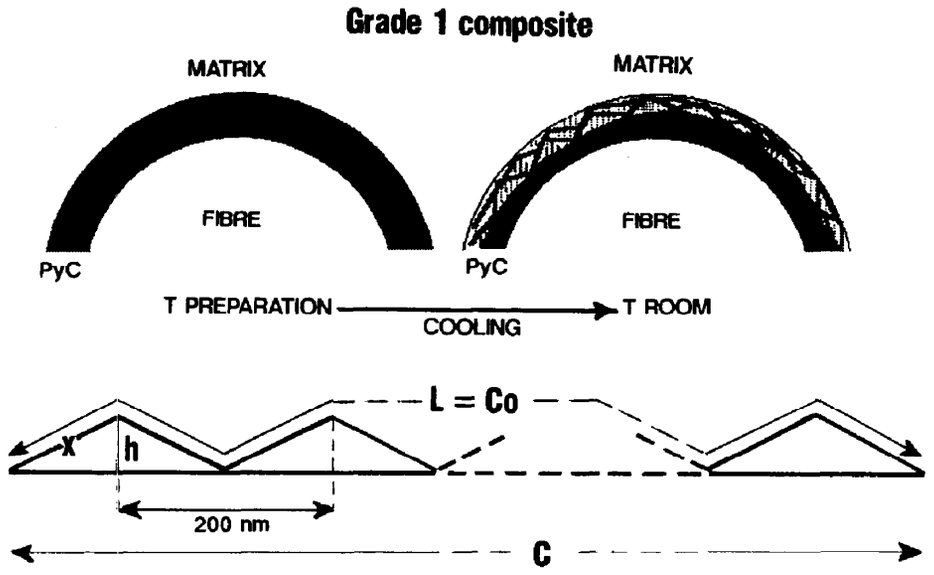

Fig. 24. Sketch of the formation mechanism of the lenticular porosity within the ANI-PyC part of the bimorphic type interphase texture, due to differences in the fibre and pyrocarbon TEC (see text).

induced by the difference in TEC is in the same range as the porosity observed. We thus believe that the lenticular porosity within Grade 1 composites is a secondary texture inherited from the cooling step rather than an intrinsic texture induced by the primary deposition step.

5 Conclusion

As previously stated for SiC/C/SiC composites, the texture of the pyrolytic carbon interphase has a major influence on the macroscopic mechanical behavior of the C/C/SiC composites. Obviously, controlling the pyrocarbon texture allows the matrix-to-fibre stress transfer to be controlled, leading to more-or-less tough composites. A common observation for tough composites is that the fibre/matrix interface has to reach a compromise: not too weak but not too strong. Whatever the texture, a pyrocarbon interphase is always efficient in dispersing the fracture energy, as compared with interphase-free C/SiC composites. Whatever the number of interfaces, the bulk behavior of the composite is mainly controlled by the weakest one. However, the efficiency is all the higher as the number of weak interfaces is high. This points out the importance of being able to order the interface strengths. For C/C/SiC composites, the interface strength may be directly related to the Van der Waals/covalent bond ratio, and increases as the ratio decreases. The 'compromise rule'—sustained by the observations—leads to the conclusion that an interface strength with a nil value is not desirable (case of the C/SiC composites), since allowing no stress transfer. In other words, some minimum strength value is necessary to get a tough composite. As compared with the interphase texture and the interface strength, other parameters such as interphase thickness or fibre topology are subordinate.

Acknowledgement

The authors thank Société Européenne de Propulsion for providing samples, results of mechanical tests, and financial support.

References

1. Christin, F., Les composites carbone–carbone–carbure de silicium: une nouvelle famille de matériaux destinés à des applications à haute température. State Thesis, Université de Bordeaux I, France, 1979.
2. Després, J.-F. & Monthioux, M., Etudes des interfaces des composites C/C/SiC. Relation avec les propriétés mécaniques. Internal Report to SEP, 1992.
3. Després, J.-F., Les interphases de carbone pyrolytique dans les composites carbone/carbure de silicium. PhD thesis, Université de Pau & des Pays de l'Adour, France, 1993.
4. Oberlin, A., Application of dark-field electron microscopy to carbon study. *Carbon*, **17** (1979) 7–20.
5. Després, J.-F. & Monthioux, M., Microtextures of interfaces related to mechanical properties in carbon fibre reinforced ceramic matrix composites. In *5th European Conference on Composite Materials Proceedings*, ed. A. R. Bunsell, J. F. Jamet & A. Massiah. EACM, Bordeaux, 1992, pp. 901–6.
6. Maniette, Y., Contribution a l'étude de phénomènes d'interphases dans des composites de carbure de silicium. PhD thesis, Université de Pau & des Pays de l'Adour, France, 1988.
7. Cojean, D., Monthioux, M. & Oberlin, A., Phénomènes interfaciaux dans des composites SiC/SiC 2D de propriétés mécaniques variées. In *Comptes-Rendus des Septièmes Journées Nationales sur les Composites*, ed. G. Fantozzi & P. Fleischmann. AMAC, Paris, 1990, pp. 103–11.

8. Cojean, D. & Monthioux, M., Microtextures of interfaces related to mechanical properties in ceramic fibre reinforced ceramic matrix composites. In *5th European Conference on Composite Materials Proceedings*, ed. A. R. Bunsell, J. F. Jamet & A. Massiah. EACM, Bordeaux, 1992, pp. 729–34.
9. Gulbransen, E. A. & Jansson, S. V. The high temperature oxidation, reduction and volatilization of silicon and silicon carbide. *Oxidation of Metals*, **4** (1972) 181–201.
10. Després, J.-F., Vahlas, C. & Oberlin, A., Chemical vapor deposition of pyrolytic carbon on polished substrates. *J. Phys. IV*, **3** (1993) 563–70.